The Application of Fluidic Sealing
in Shrouded Gas Turbine Blades

3

4 **Filip Wasilczuk[1]**
5 Institute of Fluid-Flow Machinery, Polish Academy of Sciences
6 Fiszera 14, 80-231, Gdańsk, Poland
7 fwasilczuk@imp.gda.pl
8

9 **Paweł Flaszyński**
10 Institute of Fluid-Flow Machinery, Polish Academy of Sciences
11 Fiszera 14, 80-9522222, Gdańsk, Poland
12 pflaszyn@imp.gda.pl
13

14 **Piotr Doerffer**
15 Gdańsk University of Technology
16 Narutowicza 11/12, 80-233 Gdańsk Poland
17 doerffer@imp.gda.pl
18

19 **Krzysztof Marugi**
20 Avio Polska Sp. z o.o.
21 Grażyńskiego 141, 43-300, Bielsko-Biała, Poland
22 krzysztof.marugi@avioaero.it
23

24 **Tomasz Borzęcki**
25 Avio Polska Sp. z o.o.
26 Grażyńskiego 141, 43-300, Bielsko-Biała, Poland
27 tomasz.borzecki@avioaero.it
28

29

30

31

---
[1] Corresponding author.

32   **ABSTRACT**

33   This paper presents a study conducted on a new gas turbine, designed to limit

34   leakage in the labyrinth seal. The slots in the fin are used to generate a bypass flow, which

35   obstructs the flow in the gap above the fin. The method was tested numerically and

36   experimentally beforehand using a simplified model without rotation or blade passages.

37   In this paper, the validation of the method using a model of a turbine stage is shown.

38   RANS simulations using two turbulence models – Spalart-Allmaras (SA) and k-ω EARSM

39   were conducted. Comparisons of leakage flow and stage efficiency for reference and

40   fluidic sealing configurations are presented. Fluidic sealing configuration is effective and

41   reduces the leakage flow by 13-18.5% (depending on the turbulence model). The analysis

42   of the flow structure in the seal region revealed, that the use of fluidic sealing resulted in

43   significant circumferential flow anisotropy.

44   Keywords: Labyrinth Seal, Flow Control, Leakage reduction

45

46   **1. INTRODUCTION**

47   Pollution from air travel can be reduced by increasing engine efficiency, which also

48   improves operation profitability. There are many aspects of engine operation that can be

49   investigated in order to reduce loss. However, this study is mainly focused on losses

50   resulting from leakage, which contribute up to 25% of stage losses [1]. Seal leakage

51   impacts three aspects of turbine performance. Firstly, it reduces working potential, as

52   some of the air that could work in the blade passage passes through the seal. Secondly,

53 the flow's kinetic energy is dissipated as mixing occurs in the seal. Lastly, the fluid passing

54 through the seal has a different velocity to the fluid in the main channel, thus mixing

55 occurs, leading to decreased performance in further turbine stages [2]. In the shrouded

56 blades, which are investigated in this work, labyrinth seals are used to limit the leakage

57 [3]. Labyrinth seals consist of several fins, which engage in a series of contractions that

58 obstruct the flow. The shape of those fins is optimized to reduce the leakage [4].

59 Introducing flow control in the seal region can lead to a further reduction, as shown in [5-

60 8]. Considering the widespread use of the gas turbines in aircraft, even a modest

61 reduction in leakage would have a considerable impact globally.

62   Fluidic sealing in turbine labyrinth seals was first presented in the 1950s patent by

63 Auyer [9], which used pressurized air from a compressor and injected it into the tip gap

64 of an unshrouded turbine. Smile and Paulson [10] implemented the same concept with

65 high pressure air introduced in the cavern between the fins' labyrinth seal of a shrouded

66 blade. Hilfer [11] optimized the configuration, which resulted in a 28% leakage reduction.

67 Placing the fluidic seal in the gap above the fin of the labyrinth seal was first proposed by

68 Rushton [12].

69   Subsequent research shows passive configurations of the fluidic sealing, where no

70 additional air supply is needed. In this case, the source of pressurized air is usually

71 upstream of the seal [7], where the pressure is greater than in the gap. Ghaffari [13,14]

72 presented a similar idea, but used the elevated pressure from the stagnation point at the

73 leading edge of the turbine blade.

74   The solution presented in this paper combines two important features of the

75   solutions presented in the literature review, which, to the best of the authors' knowledge,

76   has not been done before. Namely, the bypass slot is entirely incorporated within the fin

77   of the seal while at the same time being passive. The modus operandi is shown in Fig. 1.

78   In the labyrinth seal, the pressure upstream of the fin is higher than downstream of the

79   fin. Therefore, the pressure is higher at the slot inlet than the slot outlet, which drives the

80   flow through the slot. The proposed method is passive, which is an advantage and may

81   lead to an overall improvement in performance in the gas turbine stage.
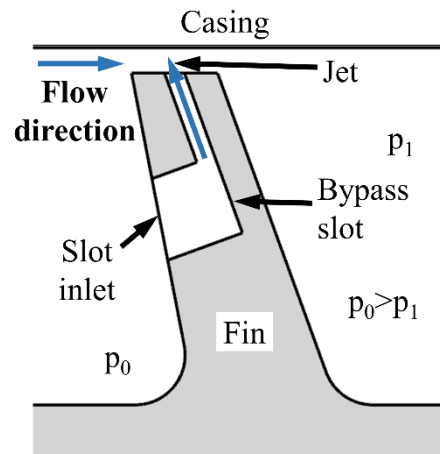
82

83   Fig. 1 Operation principle of the fluidic seal [15]

84   The experiment was conducted on a simplified, static (non-rotating), linear

85   labyrinth seal configuration of a low-pressure turbine stage [5,6,15], where various

86   configurations of the seal were placed in a wind tunnel. The pressure ratio between the

87   section's inlet and outlet was set using valves, after which the stagnation parameters,

88   mass flow at the inlet and pressure distribution in the seal were measured. A pressure

89   ratio ranging from 1.05 to 2.05 was tested to verify the design in a wide range of

   TURBO-23-1021 Wasilczuk *et al.*

90   conditions. One of the selected conditions corresponds to the pressure ratio in the design

91   point of the labyrinth seal in a turbine. However, due to experimental restrictions, the

92   ambient temperature was used instead of the elevated one. Additionally, the test section

93   allowed for the investigation of configurations with different gap heights, which reflects

94   the changing gap height present during turbine operation. However, in this paper only

95   two gap heights are presented: h=0.85s and 1.25s, where s is the thickness of the

96   reference fin.

97   The experimental results, comparing the reference case and the case with fluidic

98   sealing [5,6] show the leakage reduction of up to 16% was achieved in the latter

99   configuration.

100   As the purpose of this paper is to present turbine stage simulations, the

101   experimental data is shown only as a validation tool for the numerical model, thus not

102   many details are presented. A more inquisitive reader should refer to [5,6,15], where

103   more information, including the equipment used and measurement errors are presented.

104   The numerical simulations were carried out using the k-ω EARSM [16] and Spalart-

105   Allmaras [17] turbulence models. Both models showed satisfactory qualitative agreement

106   with the experimental data, with small quantitative differences [5,6]. The efficiency of the

107   fluidic sealing in reducing the leakage flow was proven in simulations using both

108   turbulence models. The CFD approach also showed that fluidic sealing may reduce the

109   leakage flow by up to 22%.

110   Results from the RANS simulations of simplified configuration (described in detail in

111   section 2) served as a source for a brief description of operating principles of the fluidic

112   sealing presented below. The air at the slot outlet has significant velocity, perpendicular

113   to the main flow, which constitutes an obstacle for the main flow. In addition, the

114   difference in the magnitude and direction of the velocity creates additional vortex

115   structures (Fig. 2), which are described in sections 4 and 6. Additionally, since the slot

116   does not cover the entire fin in the circumferential direction, the main flow is impacted

117   by the flow exiting the slot differently at various sections of the gap. This introduces an

118   additional non-uniformity of the flow in the gap, which then propagates into the cavern

119   between the fins. The non-uniformity causes additional mixing in this zone, which leads

120   to a higher dissipation of kinetic energy in the flow. The comparison of the flow structure

121   with and without the fluidic sealing is analyzed in detail in [6].
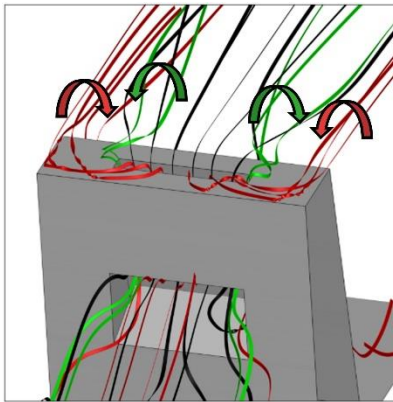
122

123   Fig. 2 The vortex structure generated by the fluidic seal, direction of vortex rotation

124   marked with arrows. Example representation based on data obtained in RANS

125   simulations [6].

126

127 **2. NUMERICAL MODEL VALIDATION**

128   Before fluidic sealing was implemented in the simulations of the turbine stage

129 model, an extensive study was conducted on the simplified model, which included

130 experimental campaign. The comparison of experimental and numerical results was used

131 to validate the numerical model. The definition of the configuration is presented in this

132 section, along the validation results.

133   Fine/Turbo Numeca code was used to simulate the flow through the labyrinth seal.

134 Steady RANS calculations were conducted, with the k-ω EARSM and Spalart-Allmaras

135 turbulence models. Perfect gas was assumed with viscosity calculated according to

136 Sutherland's law. The code uses the second order central difference spatial discretization

137 scheme with artificial dissipation, as well as the explicit Runge-Kutta numerical scheme.

138 Additionally, the Full Approximation Storage multigrid strategy, with coarse grid

139 initialization was utilized. Numerical settings are presented in Tab. 1.

140   Tab. 1 Numerical settings for performed simulations.

Parameter	Setting
Turbulence model	S-A, EARSM
Spatial discretization	2nd order central difference with artificial dissipation
Numerical scheme	Explicit Runge-Kutta
Multigrid strategy	Full Approximation Storage (3 levels)
Medium	Perfect gas
Viscosity	According to Sutherland law

141

142   The boundary conditions were set according to the measurement set up (described

143 in section 1). The stagnation pressure and temperature were set at the inlet and the static

144   pressure at the outlet. Walls were set as adiabatic. The turbulence at the inlet was not

145   measured in the experiment, so it was assumed. The turbulent viscosity ratio was set to

146   5 and the turbulence intensity to 5%. The configuration has significant contraction (10:1)

147   between the inlet and the channel leading to the labyrinth seal (which is the focus of the

148   study), followed by yet another contraction (about 10:1, depending on gap height)

149   between the channel and the gap above the fin. Thus the turbulence at the inlet does not

150   impact the flow in the seal in meaningful manner.

151   A block-structured hexahedral mesh was used, refined close to the wall to keep y+

152   at less than 2 around the seal. The selection of the final grid was preceded by a grid

153   convergence study, so that the results are grid-independent [6]. The final grid size is equal

154   to 5.8 million cells.

155   The focus of the research presented in this paper is the fluidic sealing, which is

156   created using the slots drilled in the labyrinth seal fins. The crucial geometrical features

157   of the slot such as its outlet dimensions are the same for simplified configuration and

158   stage configuration (shown in sections 4-6). The shape of the slot is a compromise

159   between its effectiveness and the manufacturing feasibility. However, in the future,

160   additive manufacturing technology will allow for more complex and optimal slot shapes.

161   The dimensions of the slot, including the inlet and outlet dimensions as well as the slot

162   inclination angle were determined using a parametric study, presented in [8], while the

163   relative dimensions of the slot are shown in Fig. 3.
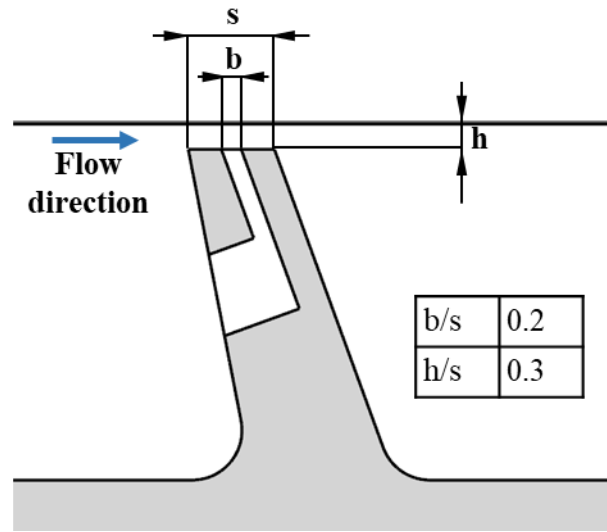
Fig. 3. Geometry of the fluidic sealing slot.

The labyrinth seal configuration was modified to allow for the design of a relatively simple test section, without sacrificing the key features of the seal flow. The simplifications neglect some secondary geometrical features, reducing the model domain to the seal only (without the blade channel) as well as disregarding rotational effects. The analysis of the impact of those simplifications is described extensively in [5]. Overall, it can be concluded, that while some of the simplifications have a non-negligible impact on the level of leakage flow, the main features of the labyrinth seal flow are conserved in the simplified model. Thus, the simplified model was deemed sufficient for proving the concept and assessing the effectiveness of proposed modifications. Nevertheless, testing of the fluidic sealing in the actual turbine configuration before it can be implemented is essential.

Figure 4 presents a comparison of the mass flow from the numerical model with the measurements in the test section, normalized by the maximum value obtained in the

TURBO-23-1021 Wasilczuk *et al.*

179   experiment. The mass flow for both turbulence models is very similar and is

180   underestimated by about 8% in the entire range. However, the trend of mass flow change

181   with rising pressure ratio is the same for experimental and numerical results. At the same

182   time, the pressure distribution at the platform (upper wall of the model) calculated using

183   both turbulence models, concurs well with the measured values. In previous studies [5,6]

184   it was established, that the leakage flow is sensitive to the turbulence model used. The

185   leakage flow highly depends on the flow area in the gap, which in turn is impacted by

186   separation bubble height. After exiting the gap the flow enters the cavern, where it is also

187   separated. It is well known, that the accuracy of the turbulence models in separated flow

188   is limited. In this case, the proposed model is considered accurate for the purpose of the

189   study. The improvement of accuracy may be obtained with LES simulations, which are

190   planned in the future.

191

a)

b)

192
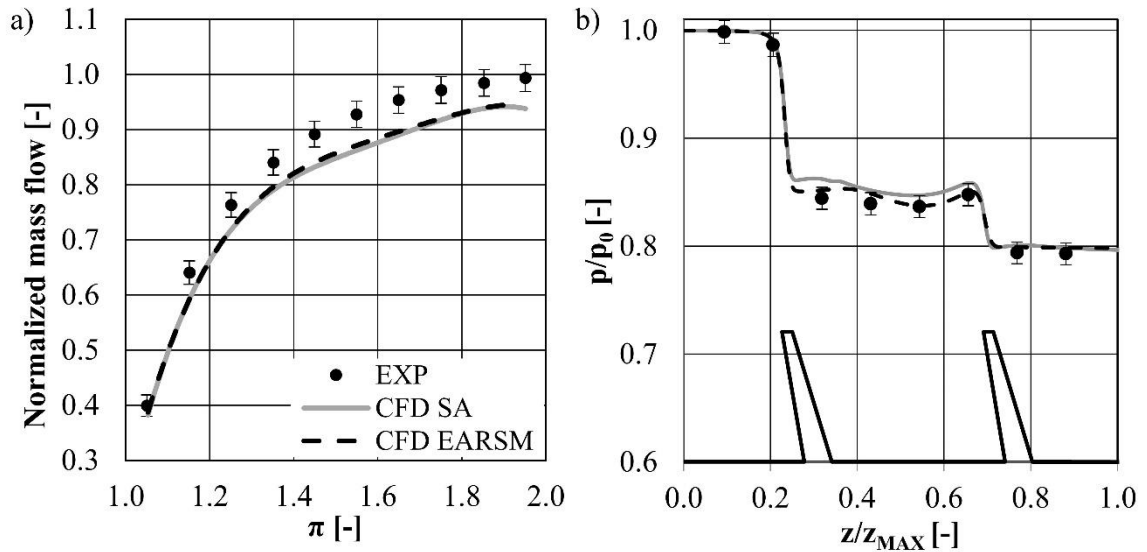
Fig. 4. Comparison of the quantities obtained in the experiment [5] and the numerical

model with two turbulence models (Spalart-Allmaras and k-ω EARSM).

Gap height = 0.85s, pressure ratio = 1.25. a) Mass flow through the seal normalized with

the maximum value in the experiment. b) Static pressure at the casing normalized by

inlet total pressure.

3. TURBINE STAGE MODEL DESCRIPTION

Turbine stage simulations used the same numerical settings as the simplified

configurations simulations, while the geometry and boundary conditions were modified.

The details of the seal configuration are protected, but key information can be

shared. Similarly to the configuration used in the experimental step, the seal in the stage

configuration has two fins, the clearance used was 0.38 of the fin thickness. However,

there are some geometrical differences between the simplified (experimental) and the

stage configuration, due to the labyrinth seal optimization conducted in the period

11   TURBO-23-1021 Wasilczuk *et al.*

207   between the experiment and the stage simulations [18]. Figure 5 presents comparison of

208   two configurations – simplified and stage. Apart from geometry differences, other

209   differences between the models that were mentioned in section 2 and discussed in detail

210   in [5] are listed in the figure.
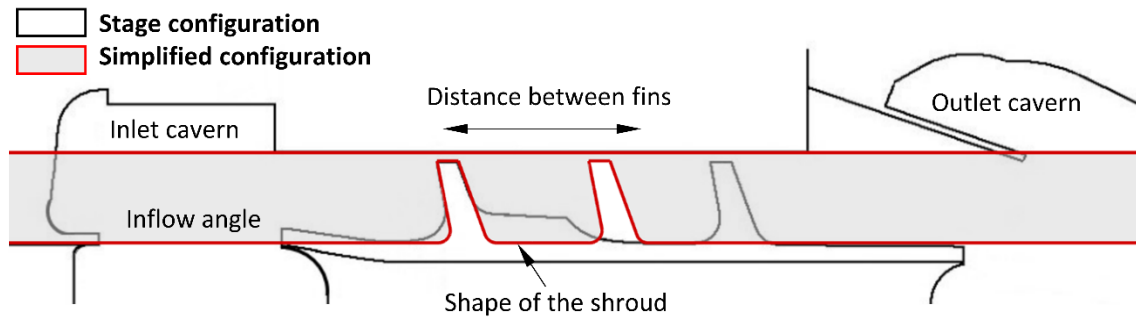
212   Fig. 5. Schematic comparison of stage and simplified configurations. Differences

213   between configurations are listed in the figure.

214   Even though the stage configuration is much more faithful representation of a real

215   turbine than the simplified configuration, there is one major difference between it and

216   the real engine – namely the honeycomb at the casing was neglected. The experimental

217   studies on the simplified test section show that the currently investigated fluidic sealing

218   is not effective when a honeycomb is used. This issue is still being researched, as the

219   honeycomb adds complexity to the case. Some of the concepts that can make the

220   configuration with fluidic sealing and the honeycomb combination effective are discussed

221   in [15]. It is important to note, that the fluidic sealing is investigated as a means to reduce

222   the leakage flow in a wide range of applications, where the clearance is small and

223   unavoidable, not only in LP turbines, where honeycombs are prevalent.

224   The stage used in simulations is defined based on the last stage of a low-pressure

225   turbine of a GEnx engine. As with the seal geometry, the details cannot be shown, but for

226   reference approximate dimensions and features are specified below. The stator consists

227   of 168 blades, while the rotor of 114 blades. The shroud radius is about 1 m, with blades

228   length of about 300 mm. The gap between the casing and the labyrinth seal roughly 1 mm.

229   The rotation rate of the rotor is 2100 RPM. The ratio of total pressure ratio at stage inlet

230   and static pressure at the outlet is equal to 1.6.

231   Two models were created with two versions of the labyrinth seal mounted on the

232   rotor blade. In the reference configuration a standard, unmodified labyrinth seal was

233   installed, while the seal of the second model included fluidic sealing slots. Apart from the

234   slots, both configurations were identical.

235   The grid for the blades channel was generated by the Autogrid/Numeca code with

236   O4H topology, which provided good quality [15,19]. The grid of the labyrinth seal (Fig. 6)

237   was created in IGG/Numeca and added to the channel grid. The grid of the labyrinth seal

238   was split into two parts, one connected to the stator grid and the one to the rotor grid

239   (see Fig. 7). The periodicity of the seal grid matches the periodicity of the blade passage.

240   Both domains - the seal and the blade passage, were connected with non-matching

241   interfaces. The non-matching connection is created using Alternating Digital Trees (ADT)

242   algorithm [20]. One side of the connection is triangulated and projected on the other side.
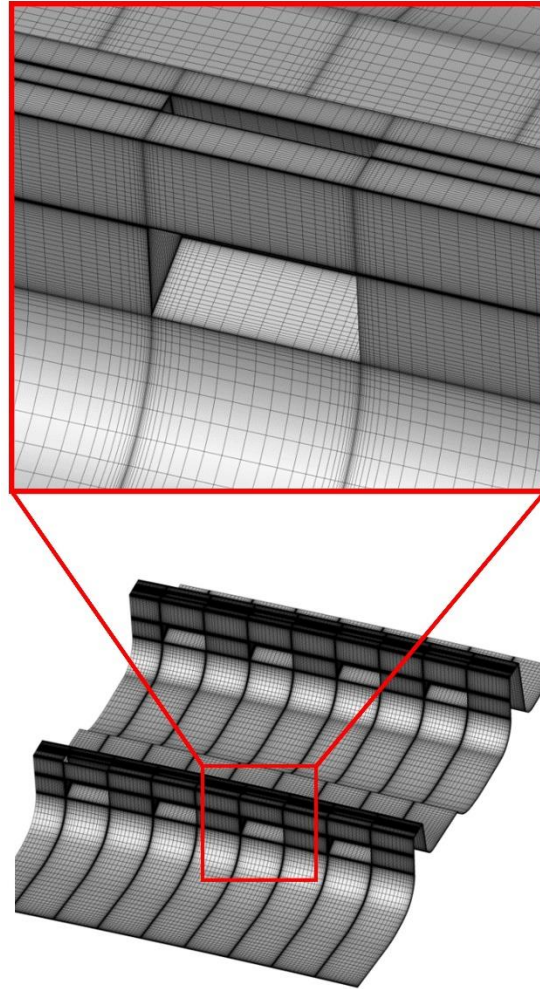
243

244   Fig. 6. Grid of the labyrinth seal.

245   The grid resolving the flow through the blades consists of two parts – rotor part and

246   stator part, connected with rotor-stator interface. Table 2 shows the grid resolution in

247   selected directions, such as radial, circumferential, pressure side (PS) and suction side (SS)

248   resolution for the blades, as well as resolution in all three directions for the seal and the

249   gap above the fin.

250

251 Tab. 2 Resolution of the computational grid in selected directions

	Circumferential (X)	Radial (Y)	Axial (Z)	
Gap	364	36	112	
Seal	364	128	412	
Stator	64	108	112 (PS)	232 (SS)
Rotor	125	108	116 (PS)	300 (SS)

252

253 Appropriate grid resolution on the side walls of the slot leads to a significant number

254 of elements in the circumferential direction. This causes the grid to be large. Introducing

255 a non-matching interface (Fig. 7) allows for the reduction of circumferential resolution in

256 the inlet and outlet caverns of the seal, where refinement is not required. As a result, the

257 mesh size can be significantly reduced. Still, the final grid consists of 21 million cells, out

258 of which about 16.5 million are located in the labyrinth seal zone.
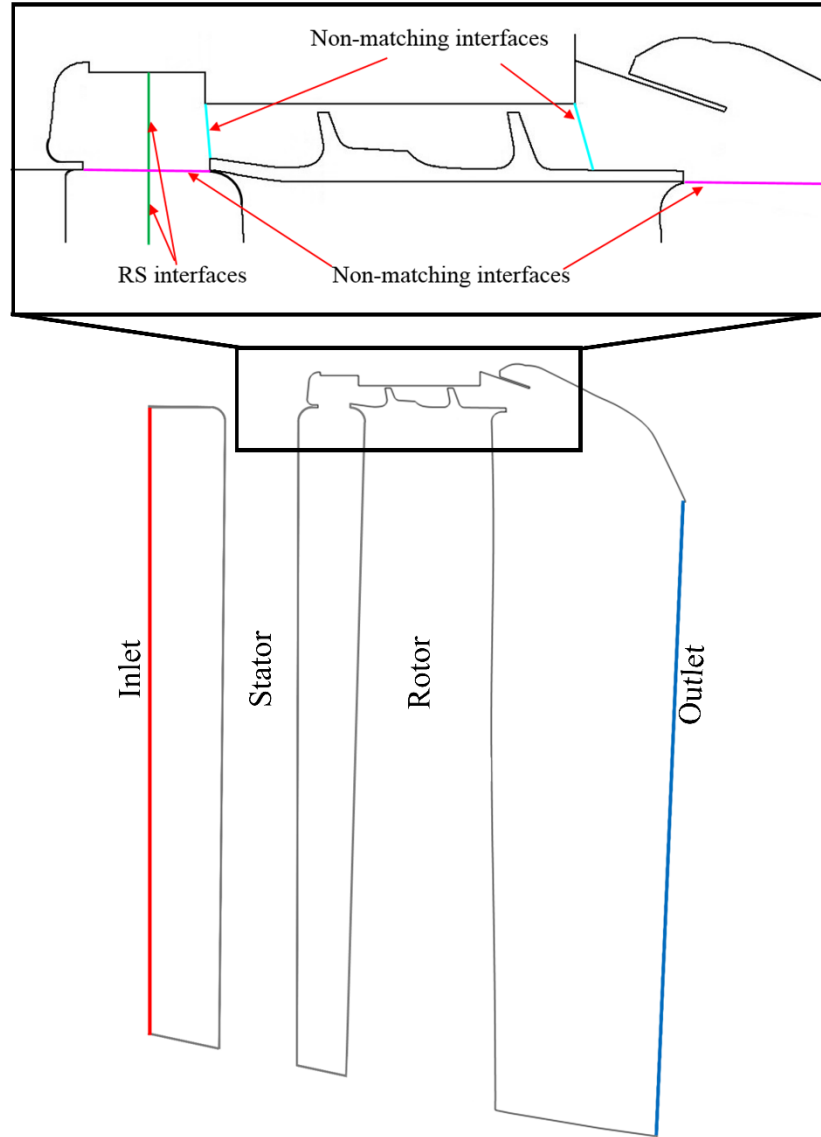
259

Fig. 7. A numerical model of a turbine stage with the labyrinth seal, with marked

boundary conditions and interfaces used.

262

263

264   The boundary conditions were a result of a 2D, throughflow simulation of the entire

265   engine. The distribution along the turbine radius of total pressure p_1 (average ~60 kPa),

266   temperature T_1 (average ~700K) and flow direction was specified at the inlet, upstream

267   of the stator. Turbulence quantities were not known, therefore they were assumed: the

268   turbulent viscosity ratio was at 10 and turbulence intensity at 5%. However, the

269   turbulence quantities at the inlet should not impact the flow in the labyrinth seal, since

270   before reaching it, the flow passes through the turbine stator. At the outlet, a static

271   pressure level of 38 kPa was imposed at the radius of the hub with the hub-to-shroud

272   pressure profile calculated according to the radial equilibrium conditions [21]. The speed

273   of rotation is 2100 RPM.

274   As for the simplified seal configuration the Numeca/FineTurbo code, which is widely

275   used for turbomachinery simulations, was applied. Simulations were carried out for the

276   steady flow and the full non-matching mixing plane (with the conservation of fluxes) for

277   stator/rotor interface. Additionally, the field variables on one side of the interface were

278   circumferentially averaged and applied to the other side.

279

280   **4. TURBINE STAGE MODEL COMPARED TO SIMPLIFIED CONFIGURATION**

281   As mentioned before, the concept of fluidic sealing in a turbine labyrinth seal was

282   proved effective for simplified, non-rotating configurations. However, due to the

283   simplifications used in the model, additional simulations with fluidic sealing applied to a

284 turbine stage configuration were performed. This made it possible to check the concept
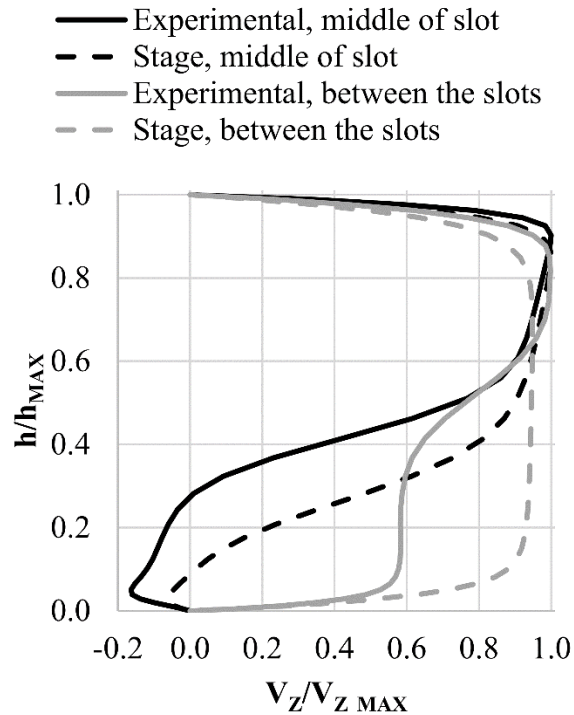
285 in target conditions.

286   Ideally, the numerical model for the turbine stage with the labyrinth seal would be

287 validated against the experimental data. However, even conducting the experiment with

288 just the rotating labyrinth seal (without the blade channel) would be too complex a task

289 and currently beyond available options. Therefore, despite the number of differences

290 between the simplified case and the turbine stage configuration, a qualitative comparison

291 is presented to show that the main features of the labyrinth seal and fluidic sealing flow

292 characteristics are maintained. The differences between cases include (Fig. 5):

293   • Geometry

294   • Rotational velocity

295   • Boundary conditions

296   Obviously, the simplified case (the static test section) did not include rotational

297 velocity, which is present in stage simulations. While the absolute-to-static pressure ratio

298 differs between the cases (due to the significant dynamic pressure from rotational

299 velocity), the static-to-static pressure ratio in the seal is the same for both cases (the

300 dynamic pressure from axial velocity at the seal inlet is negligible). It is worth noticing,

301 that in the stage simulations, the pressure ratio in the seal is not prescribed, but rather a

302 result of the blade passage solution. The rotational velocity in the seal is significant for

303 the stage simulations, while for the experimental setup it is non-existent. Moreover, in

304   the simplified case, an ambient temperature was set, while in the stage simulations the

305   inlet temperature was derived from the real turbine.

306   Because of these differences, a direct comparison of the mass flows obtained in the

307   experiment and the stage simulations is not valid. Instead, a qualitative comparison of the

308   flow structure created by the jet exiting the fluidic sealing slot, is shown in the following

309   section. The axial velocity profiles (normalized with the maximum value) at two traverses

310   located at the outlet of the gap above the fin are presented in Fig. 8. The first traverse is

311   located in the middle of the slot (black lines) and the second one between the neighboring

312   slots (grey lines). While the flow structure for the stage configuration will be investigated

313   in more detail in section 6, it is worth noting the similarities and differences between the

314   stage and experimental configurations. In both cases, the average velocity is greater in

315   the area between the slots than in the zone where the jet exits the slot, causing a velocity

316   reduction. In the space in the gap close to the slot, the velocity field is very similar in both

317   cases. Downstream of the gap, the flow in the stage configuration is subject to rotational

318   effects (discussed in more detail below), thus differences arise. In both cases, in the area

319   between the slots, the separation in the gap which is present in the reference

320   configurations (not shown here), is reduced when fluidic sealing is used. In the stage

321   configuration, the velocity is almost constant across the gap (excluding the boundary

322   layers), while in the experimental configuration it is variable. This happens, because the

323   complex vortical structure generated by the jet in the simplified configuration is disturbed

324   by significant rotational velocity.

Experimental, middle of slot
Stage, middle of slot
Experimental, between the slots
Stage, between the slots

325

Fig. 8. Profile of the normalized axial velocity in the first gap for two traverses in the

experimental and stage configurations.

Fig. 9 presents the streamlines of relative velocity. The jet exiting the slot (black

streamlines) creates a fluidic seal, that obstructs the main flow. Additionally, the air

exiting the slot in a sideways direction generates stream-wise vortices. They are present

in both of the configurations shown, however in the stage configuration the vortices are

much less developed and more thinly spread in the circumferential direction. In the

simplified configuration one can also notice that the air exiting from the front part of the

slot (red streamlines) enters the separation vortex and later forms a counter-rotating

vortex in the area between the slots. This flow feature is not present in the stage

configurations, as the separation is less pronounced due to the significant rotation

337 velocity of the fin. Moreover, the flow structures generated by mass transport in the

338 tangential direction are subject to disturbance caused by the rotational velocity of the fin.
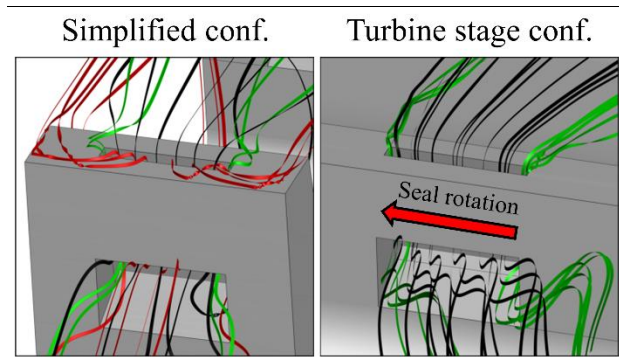
339

340 Fig. 9. Comparison of vortex structure in experimental and stage configurations.

341 Overall, some of the flow features, such as velocity reduction in the area of the slot

342 and the generation of streamwise vortices at the side edges of the slot, are similar in both

343 presented configurations. The flow in the area between the slots has a higher average

344 velocity in both configurations, however the velocity profile in the gap differs.

345 Additionally, the counter rotating vortices in the area between the slots are not present

346 in the stage configuration, contrary to the experimental configuration.

347

348 **5. TURBINE STAGE MODEL RESULTS**

349 The investigation of the impact of fluidic sealing on the flow through a labyrinth seal

350 in the turbine stage is split into two parts. Firstly, the change in global parameters, such

351 as leakage flow and stage efficiency is presented. This is followed by a comparison of the

352 flow structure existing in the reference case and the case with the fluidic seal. This is

353 helpful in assessing the reasons for the change in the global parameters.

354   The implementation of fluidic sealing in the labyrinth seal of a turbine stage reduces

355   the leakage flow. The predicted reduction depends on the turbulence model used in the

356   simulation. For k-ω EARSM it is equal to 13%, while for Spalart Allmaras it is 18.5%

357   (Fig. 10). This difference is caused by different separation sizes in the gap above the fin,

358   predicted by these models, which is discussed in the next paragraph. Interestingly, the

359   reduction of the leakage flow leads to a slight increase in the blade passage flow.
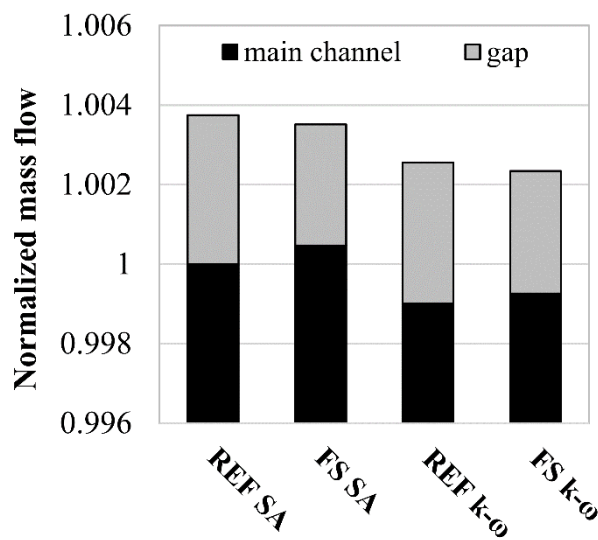
360

361   Fig. 10. Mass flow for reference and fluidic seal configuration, normalized with the value

362   of main channel flow for reference Spalart Allmaras case.

363

364   Decreasing leakage leads to an increase in stage isentropic total to total efficiency,

365   which is defined as:

$$\eta = \frac{1 - \dfrac{T_2}{T_1}}{1 - \left(\dfrac{p_2}{p_1}\right)^{\frac{\kappa - 1}{\kappa}}} \qquad (1)$$

366   Where:

367   p_1, p_2 – total pressure at inlet and outlet

368   T_1, T_2 – total temperature at inlet and outlet

369   κ – heat capacity ratio

370

371   Of course, the isentropic efficiency increase is also dependent on the turbulence

372   model and is equal to 0.065% and 0.04% for k-ω EARSM and Spalart-Allmaras respectively.

373   This efficiency increase is not large, however there are several reasons why the concept

374   is worth further investigation. Firstly, in the case of the investigated stage, the blades are

375   very long compared to the gap size, so the leakage flow is only 0.3% of the total mass

376   flow. Therefore, even a significant leakage reduction impacts the stage efficiency only

377   marginally. In the future, the concept will be tested further using blades with different

378   lengths. Additionally, the slots that generate fluidic sealing were not optimized to operate

379   in the rotating framework. In fact, as the aim of the research was to test the viability of

380   the fluidic sealing as a leakage reduction device, the geometry of the slot was not

381   optimized. Last but not least, the presented efficiency is calculated for one stage only,

382   implementing fluidic sealing in more stages would likely bring further gains, since the

383   leakage would be reduced at each stage. Leakage losses are not only connected with loss

384   of working potential, which is could be treated as isolated to the single stage, but also the

385   mixing losses that impact other stages.

386

387 **6. FLOW FIELD ANALYSIS**

388   A flow field analysis was conducted to study the reason behind the leakage

389   reduction when the fluidic sealing was used. A comparison of the flow structure in the

390   reference and the fluidic sealing cases is presented in Figs. 11-12. Figure 11 shows the

391   contour of the axial velocity in the meridional cross-section. Even though there is some

392   circumferential non-uniformity in the reference case, it is minor in comparison to the

393   fluidic sealing case. Therefore, only one cross-section for the reference case is shown,

394   while for the fluidic sealing case, the cross-sections in the middle of the slot as well as in

395   the area between the slots are shown. In Fig. 12, the axial velocity distribution in the

396   constant radius surface is shown. This surface is located in the middle of the tip gap. The

397   location of the fins and slots (in the fluidic sealing case), as well as the rotation direction,

398   is marked in the figure. In the cross section, recirculation zones with very low velocity in

399   the cavities upstream and downstream of the seal can be noticed.

400
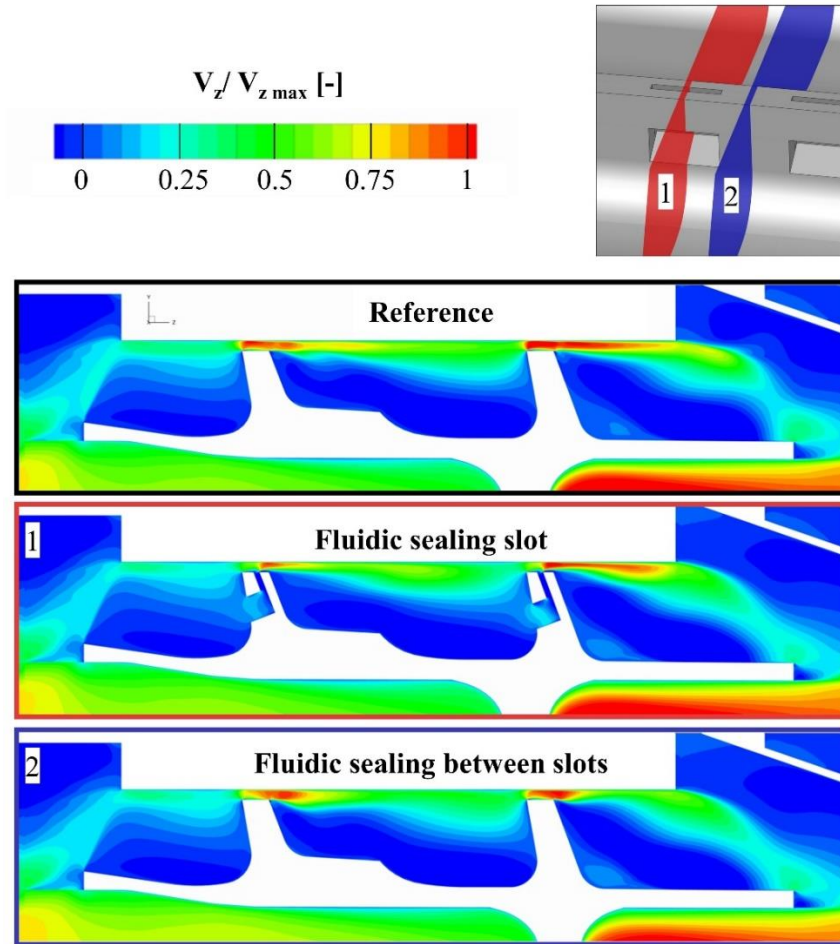
Fig. 11. Normalized axial velocity for the reference case and the two cross-sections of the fluidic sealing case.

In the reference case, the flow accelerates in the gaps above the fins. This leads to the creation of the high velocity zone that goes into the area between the fins (which can be seen in Fig. 11). A similar zone is created above the second fin. In Fig. 12, the non-uniformity of velocity in the circumferential direction can be noticed. The flow through the blade passages is not uniform, which impacts the conditions at the inlet and outlet of the seal. Additionally, the slight impact of the computational grid can be noticed. As mentioned before, both the reference and fluidic sealing grids are very similar, with the

410   only difference being the presence of slots. In the fluidic sealing case, the grid was created

411   so that the boundary layer inside the slots was properly resolved. This means that the grid

412   refinements which are close to walls propagate in an axial direction which causes visible

413   non-uniformity in the circumferential direction. This effect also exists in the reference

414   grid, since both grids are almost the same. Nevertheless, the non-uniformity of the flow

415   in the reference case, resulting from the grid resolution, is minor and does not

416   significantly affect the results. In fluidic sealing case, the periodic high velocity zones

417   downstream of the second fin have a different periodicity than the grid blocks.

418
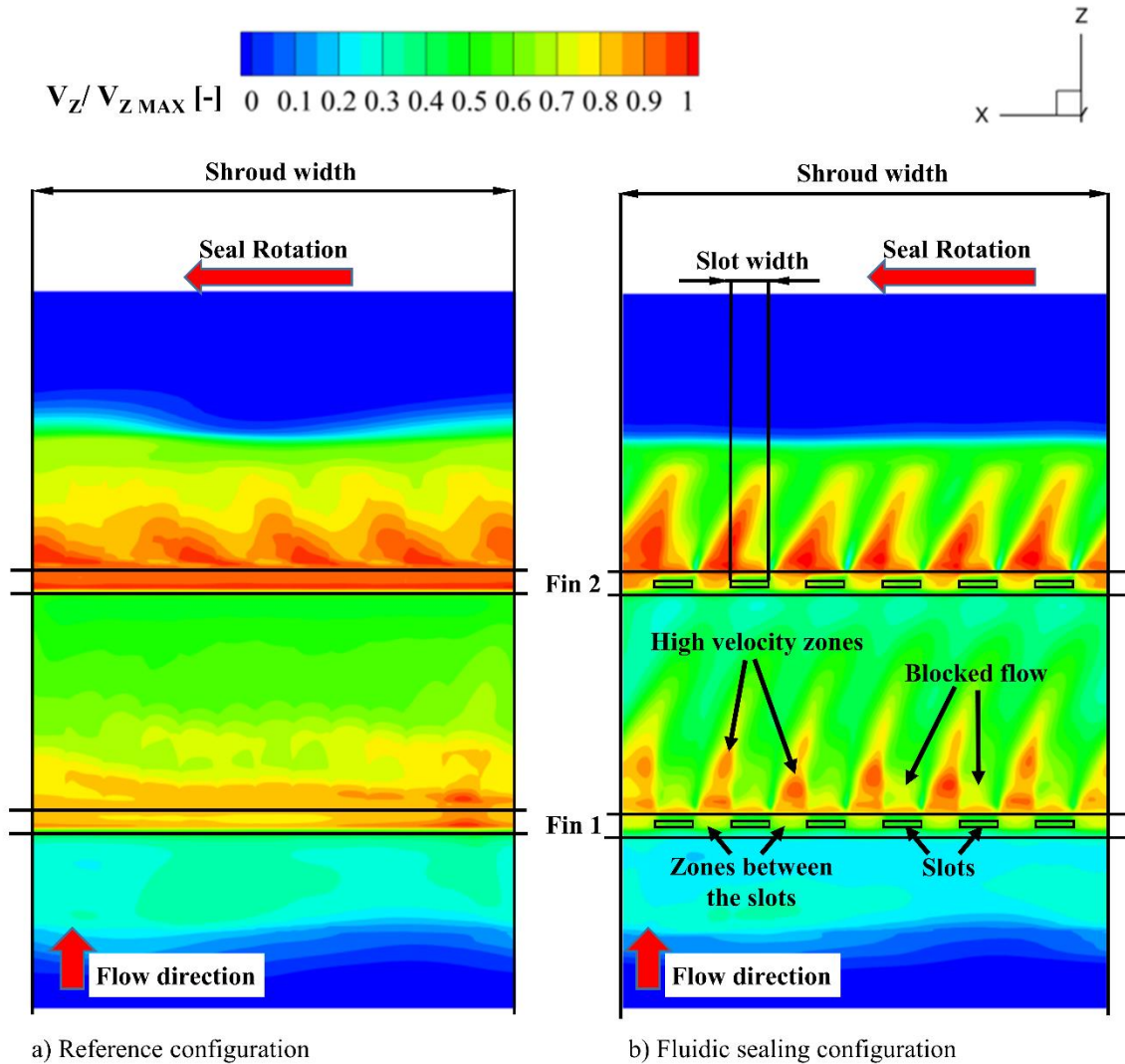
a) Reference configuration   b) Fluidic sealing configuration

419

420 Fig. 12. Normalized axial velocity for the reference and the fluidic sealing case for a

421 constant radius cross-section.

422   Implementing fluidic sealing significantly impacts the flow in the gap above the fins.

423 Strong circumferential non-uniformity is present, with two distinct flow patterns. Firstly,

424 in the zones above the slots, the high velocity is significantly diminished in comparison

425 with the reference case. The main flow in that region is blocked and pushed upwards by

426 the jet exiting the slots. Moreover, the very presence of the jet causes the expansion of

427   the high velocity zone in the cavern to be less prevalent than in the reference case (Fig. 11,

428   cross section 1).

429   On the other hand, a part of the flow blocked by the jets exiting the slots, passes

430   the gap through the zone between the slots. This increases the maximum velocity there

431   and the size of the high velocity zone (Fig. 11, cross section 2). In contrast to the zone

432   above the slots, the flow exiting the gap between the slots expands more in the cavern

433   than in the reference case. One can easily notice in Fig. 12, that the high velocity zones

434   created between the slots, enter the cavern between the fins and bend in the opposite

435   direction to the rotation. This is a result of rotation. The circumferential velocity

436   component in the gap is almost equal to the rotation velocity of the seal, therefore, the

437   shape of the high velocity zones in the gap is not changed. At the same time, the

438   circumferential velocity in the cavern, between the fins and downstream of the second

439   fin is lower than the rotation velocity of the seal. Thus, in the rotating frame of reference,

440   the high velocity zone seemingly bends in the opposite direction to the rotation.

441   In addition, the velocity exiting the seal is slightly more uniform than in the

442   reference case. This is caused by increased mixing due to the high non-uniformity of the

443   flow in the circumferential direction. A more uniform flow at the outlet may be beneficial

444   since mixing occurs between the flow exiting the seal and the blade passage flow.

445   However, this aspect should be further investigated.

446   In the non-rotating framework, the air exits the slots in a direction which is aligned

447   with the main flow, but also with the sides of the slot. When the seal rotates, it has an

448   additional circumferential component. The superposition of those two effects results in

449   non-symmetric flow in the gap, which can be observed in Fig. 13. On the one side of the

450   slot, where the direction of the velocity exiting the slot matches that of the

451   circumferential velocity, there is a local speed-up. On the opposite side of the slot, the

452   circumferential velocity is reduced by the velocity of the flow exiting the slot. This

453   promotes additional mixing and may be one of the reasons for more overall flow

454   uniformity at the exit of the seal.

455
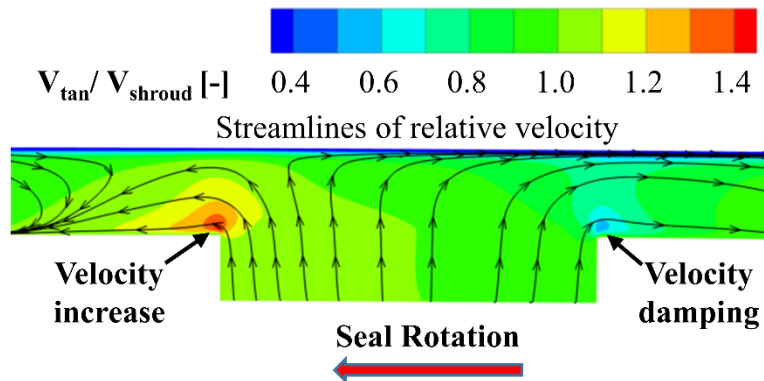
456

457   Fig. 13. Contour of circumferential velocity, normalized by the velocity of shroud rotation.

458   Streamlines (in plane) in rotating frame.

459

460   **7. CONCLUSIONS**

461   This new concept for fluidic sealing in labyrinth seals, which was previously tested

462   only in simplified conditions, was implemented in turbine stage simulations. As in the

463   simplified configurations shown in [5,6], the fluidic sealing proved to be effective in

464   reducing the leakage flow. The reduction predicted by the simulations differs, depending

465 on the turbulence model used, with 18.5% reduction obtained for Spalart Allmaras and

466 13% for k-ω EARSM. Evaluation of the stage isentropic efficiency shows improvement by

467 0.065% and 0.04% for k-ω EARSM and Spalart-Allmaras.

468   The flow structure in the reference and fluidic sealing configurations was compared.

469 The comparison revealed that the jet exiting the slots blocks the flow and leads to

470 significant circumferential flow non-uniformity. This promotes mixing, which in turn

471 increases flow resistance, eventually leading to a decrease in leakage flow.

472

473 **8. FURTHER WORK**

474   Since the fluidic sealing concept has proven to be viable, further steps can be taken

475 in order to assess its full potential, as well as to tackle possible implementation

476 challenges.

477   Firstly, the shape of the fluidic sealing slot used in this study was not optimized with

478 rotating machinery in mind. Therefore, the concept could be more efficient if the slots

479 were a different shape and were inclined in a circumferential direction.

480   The leakage reduction and stage efficiency gain resulting from the use of fluidic

481 sealing should be also assessed for different stages of the turbine and shorter blades. Such

482 a study would show whether the gains achieved in the entire turbine are significant

483 enough to warrant further investigation.

484   Additional analyses, regarding material strength and possible manufacturing

485   techniques should be performed. This would allow for a more precise selection of

486   optimization constraints for the slot. This may also lead to an improvement in efficiency.

487   Last but not least, an experimental campaign using a rotating seal could be

488   conducted to validate the numerical model in a more robust manner. This would

489   definitely illustrate whether or not the concept is viable in rotating seals.

490

496

497   **11. NOMENCLATURE**

498

b	Size of the slot in axial dimension
h	Gap height
p	Pressure
p_1	total pressure at inlet
p_2	total pressure at outlet
T_1	total temperature at inlet
T_2	total temperature at outlet
s	Thickness of the fin of the seal
y+	Non dimensional wall distance
V_{tan}	Tangential velocity
V_{shroud}	Velocity of the shroud
V_z	Axial velocity
z	Axial dimension
κ	heat capacity ratio
π	Inlet to outlet pressure ratio
CFD	Computational Fluid Dynamics
FS	Fluidic Sealing
HP	High pressure
k-ω EARSM	k-ω Explicit Algebraic Reynolds Stress turbulence model
LP	Low pressure
PS	Pressure side
RANS	Reynolds Averaged Navier Stokes
REF	Reference case (without modifications)
RPM	Revolutions per minute

RS	Rotor-Stator
SA	Spalart-Allmaras turbulence model
SS	Suction side

499 **12. REFERENCES**

500 [1] Pfau, A., 2003, "Loss Mechanisms in Labyrinth Seals of Shrouded Axial Turbines", PhD

501 Dissertation, ETH Zurich, Zurich, Switzerland.

502 [2] Kim S., Kim K., Son C., 2019 "Three-dimensional unsteady simulation of a multistage

503 axial compressor with labyrinth seals and its effects on overall performance and flow

504 characteristics", *Aerospace Science and Technology,* 86 (2019), pp. 683-693, DOI:

505 https://doi.org/10.1016/j.ast.2019.01.055.

506 [3] Denton J.D., 1993, "Loss mechanisms in turbomachines, *ASME J. Turbomach*. 115(4)

507 (1993) 621, https://doi.org /10.1115 /1.2929299.

508 [4] Lin, Z., Wang, X., Yuan, X.,. Shibukawa N., Noguchi T., 2015, "Investigation and

509 improvement of the staggered labyrinth seal" *Chin. J. Mech. Eng*. 28 (2), pp. 402-408,

510 https://doi.org/10.3901.

511 [5] Wasilczuk F., Flaszyński P., Kaczyński P., Szwaba R., Doerffer P., Marugi K., 2021 "Air

512 curtain application for leakage reduction in gas turbine shroud sealing", *Aeropace Science*

513 *and Technology*, 112, https://doi.org/10.1016/j.ast.2021.106636

514 [6] Wasilczuk F., Flaszyński P., Kaczyński P., Szwaba R., Doerffer P., Marugi K., 2021,

515 "Passive Reduction of Leakage by Transverse Jet", *J Fluids Eng – Transactions of the ASME*,

516 143

517 [7] Turnquist, N. A., Bruce, K. L., Cerretelli, C., Tourigny J. E., 2009, "Fluidic sealing for

518 turbomachinery", US patent No. 8052375B2, USA.

519 [8] Wasilczuk, F., Flaszynski P., Pyclik L., and Marugi K., 2021, "Feasibility Study of Fluidic

520 Sealing in Turbine Shroud" *Materials,* 14, no. 13: 3477.

521 https://doi.org/10.3390/ma14133477

522 [9] Auyer, E. L., 1954, "Dynamic sealing arrangement for turbomachines," US patent No.

523 2,685,429, USA.

524 [10] Smile, H. J. and Paulson E. E., 1960, "Pressurized seal," US patent No. 2963268, USA.

525 [11] Hilfer M., Hogg S., Ingram G., 2015, "Experimental Validation of a Curtain Type Fluidic

526 Jet Seal on a Turbine Rotor Shroud," Proceedings of the ASME Turbo Expo 2015: Turbine

527 Technical Conference and Exposition. Volume 5C: Heat Transfer. Montreal, Quebec,

528 Canada. June 15–19, 2015, ASME Paper No. GT2015-42624,

529 https://doi.org/10.1115/GT2015-42624.

530 [12] Rushton, G. J., 2007, "Seal arrangement" US patent No. 7238001B2, USA.

531 [13] Ghaffari, P. and Willinger, R., 2016, "On the Impact of Passive Tip-Injection on the

532 Downstream Flow Field of a Shrouded LP-Turbine: CFD and Experimental Results,"

533 Proceedings of the ASME Turbo Expo 2016: Turbomachinery Technical Conference and

534 Exposition. Volume 2B: Turbomachinery, Seoul, South Korea. June 13–17, 2016. ASME

535 Paper No. GT2016-56196, https://doi.org/10.1115/GT2016-56196.

536   [14] Ghaffari P. and Willinger R., 2015, "Preliminary Investigation of Passive Tip-Injection

537   in a Linear Turbine Cascade.", ETC Paper No. 205, 11th European Turbomachinery

538   Conference, Madrid, Spain, 2015

539   [15] Wasilczuk F., 2020, "Fluidic Control of Shroud Leakage Flow in Gas Turbine", PhD

540   Thesis, IMP PAN, Gdańsk, Poland

541   [16] Menter F., Garbaruk A., Egorov Y., 2012, "Explicit algebraic Reynolds stress models

542   for anisotropic wall-bounded flows", *Progress in Flight Physics* 3 (2012) 89-104,

543   https://doi.org/10.1051/eucass/201203089

544   [17] Spalart, P. R. and Allmaras, S. R., 1992, "A one-equation turbulence model for

545   aerodynamic flows", AIAA 30th Aerospace Sciences Meeting and Exhibit 06 January 1992

546   - 09 January 1992 Reno, NV, USA, https://doi.org/10.2514/6.1992-439.

547   [18] Szymański, A., Wróblewski, W., Frączek, D., Bochon, K., Dykas, S., and Marugi, K. 2018

548   "Optimization of the Straight-Through Labyrinth Seal With a Smooth Land." *ASME J Eng*

549   *Gas   Turbines   Power*.   December   2018;   140(12):   122503.

550   https://doi.org/10.1115/1.4040767

551   [19] Numeca, 2014, "Theoretical Manual", November, Numeca, 2014.

552   [20] Bonet, J. and Peraire, J. (1991), An alternating digital tree (ADT) algorithm for 3D

553   geometric searching and intersection problems. Int. J. Numer. Meth. Engng., 31: 1-17.

554   https://doi.org/10.1002/nme.1620310102

555   [21] Wu, C.-H., & Wolfenstein, L., 1950, "Application of radial-equilibrium condition to

556   axial-flow compressor and turbine design.", NACA Report No. 955

557

558   **13. Table caption list**

559   Tab. 1 Numerical settings for performed simulations.

560   Tab. 2 Resolution of the computational grid in selected directions

561

562   **14. Figure caption list**

563   Fig. 1 Operation principle of the fluidic seal [15]

564   Fig. 2 The vortex structure generated by the fluidic seal, direction of vortex rotation

565   marked with arrows. Example representation based on data obtained in RANS simulations

566   [6].

567   Fig. 3. Geometry of the fluidic sealing slot.

568   Fig. 4. Comparison of the quantities obtained in the experiment [5] and the

569   numerical model with two turbulence models (Spalart-Allmaras and k-ω EARSM). Gap

570   height = 0.85s, pressure ratio = 1.25. a) Mass flow through the seal normalized with the

571   maximum value in the experiment. b) Static pressure at the casing normalized by inlet

572   total pressure.

573   Fig. 5. Schematic comparison of stage and simplified configurations. Differences

574   between configurations are listed in the figure.

575   Fig. 6. Grid of the labyrinth seal.

576   Fig. 7. A numerical model of a turbine stage with the labyrinth seal, with marked

577   boundary conditions and interfaces used.

578   Fig. 8. Profile of the normalized axial velocity in the first gap for two traverses in the

579   experimental and stage configurations.

580   Fig. 9. Comparison of vortex structure in experimental and stage configurations.

581   Fig. 10. Mass flow for reference and fluidic seal configuration, normalized with the

582   value of main channel flow for reference Spalart Allmaras case.

583   Fig. 11. Normalized axial velocity for the reference case and the two cross-sections

584   of the fluidic sealing case.

585   Fig. 12. Normalized axial velocity for the reference and the fluidic sealing case for a

586   constant radius cross-section.

587   Fig. 13. Contour of circumferential velocity, normalized by the velocity of shroud

588   rotation. Streamlines (in plane) in rotating frame.

589